A Non-Contact-Type RF MEMS Switch for 24-GHz Radar Applications

Jaehong Park, Eun Sub Shim, Wooyeol Choi, Youngmin Kim, Youngwoo Kwon, *Senior Member, IEEE*, and Dong-il Cho, *Member, IEEE*

***Abstract*—This paper presents the design, fabrication, and measurement results for a novel non-contact-type radio-frequency (RF) microelectromechanical systems switch for 24-GHz radar applications. The proposed switches are free from unavoidable microwelding and stiction problems in other contact types, which in turn guarantee high reliability and long lifetime. The developed switch is a capacitive shunt type using a variation of the capacitance between the signal line and ground lines. The capacitance is precisely regulated by comb-drive actuators. This concept is simple, but the design requires a large and precise mechanical motion. In addition, for a low-loss switch structure, an air bridge with a large air gap is required. Therefore, the selective silicon-on-insulator process, based on the sacrificial bulk micromachining process, is designed for this switch fabrication. First, large insulating supports are fabricated 60 μm below the wafer surface, and then, the RF switch is fabricated on these insulating supports. The measured actuation voltage is 25 V, and the actuation stroke is 25 μm. The switching times are 8 ms in the OFF to the ON state and 200 μs in the ON to the OFF state. In the RF characteristic measurements, the insertion loss without the long coplanar waveguide line loss is 0.29 dB and the isolation is 30.1 dB at 24 GHz. The bandwidth is relatively narrow, and the isolation is 25 dB or better in the range of 23.5–29 GHz. The reliability test for the switch was performed 10^9 times with 18-mW RF power. We observed no mechanical failure or RF performance degradation. A power handling capacity of 0.9 W with a hot-switch condition was achieved. [2007-0183]**

***Index Terms*—Non-contact-type, radio-frequency (RF) microelectromechanical systems (MEMS) switch, sacrificial bulk micromachining (SBM) process, selective silicon-on-insulator (SSOI) process, variable capacitors.**

I. Introduction

SINCE THE early 1980s, technological advances in the microelectromechanical systems (MEMS) field have been truly impressive, and they have been used in inertial measurement applications, bio applications, radio-frequency (RF) applications, and optical communication applications. In particular, RF MEMS switches are one of the essential components in wireless communication systems and radar systems [1], [2]. Traditional RF signal switching has been realized using p-type intrinsic n-type diode and GaAs metal–semiconductor field-effect-transistor- or junction-field-effect-transistor-based semiconductor switches. However, these semiconductor switches have poor performance compared with RF MEMS switches. The advantages of MEMS switches over the semiconductor switches are their low insertion loss, high OFF-state isolation, and low power consumption. On the other hand, the reliability issues of MEMS switch are the major concerns for long-term applications and commercialization [2]–[4].

TABLE I
TYPICAL RELIABILITY PROBLEMS OF THE CONTACT-TYPE SWITCHES

Switch type	Problems
Metal contacting switch	- Increasing contact resistance - Microwelding phenomenon
Capacitive coupling switch	- Stiction between the dielectric layer and the metal - Charge injection and charge trapping in the dielectric layers

After the first demonstration of micromachined membrane switch in 1979, many contact-type RF MEMS switches have been developed using various actuation designs, including electrostatic, electromagnetic, electrostatic–electromagnetic, electric–thermal, and piezoelectric actuators [5]–[14]. Such switches, from a switch contact perspective, are categorized into metal contacting and capacitive coupling switches. The metal contact switch uses a metal direct contact to achieve an ohmic contact between two metal electrodes. The capacitive coupling switch has a thin dielectric film and an air gap between the two metallic contact surfaces. The air gap is electromechanically adjusted to achieve a capacitance change between the up and down states. However, the reliability of these switches is limited by microwelding and stiction problems in the contact areas. In the metal contacting switch, the direct contact between the two metal layers causes increasing contact resistance and a microwelding problem after repeated actuations. In addition, the stiction between the dielectric layer and the metal, due to the large contact area of the switch, dominates the reliability of the capacitive coupling switch. The major stiction force is due to the charge injection and charge trapping in the dielectric layers. It can cause the switch to either stick in the down-state position or result in an increase in the pull-down voltage [2]–[4], [15]. Typical reliability problems of a contact-type switch are summarized in Table I.

In order to solve these problems, we have proposed a non-contact-type RF MEMS switch. In the present configuration, the microwelding and stiction problems in the contact switches

Manuscript received July 23, 2007; revised July 30, 2008. First published January 20, 2009; current version published February 4, 2009. This work was supported by the Automotive Component Base Technology Projects sponsored by the Korea Ministry of Commerce, Industry, and Energy. An earlier version of this paper was presented at the 2007 IEEE MTT-S International Microwave Symposium, June 7, 2007, Honolulu, Hawaii. Subject Editor K. E. Petersen.

The authors are with the School of Electrical Engineering and Computer Science, Seoul National University, Seoul 151-742, Korea (e-mail: dicho@snu.ac.kr).

Color versions of one or more of the figures in this paper are available online at http://ieeexplore.ieee.org.

Digital Object Identifier 10.1109/JMEMS.2008.2011124

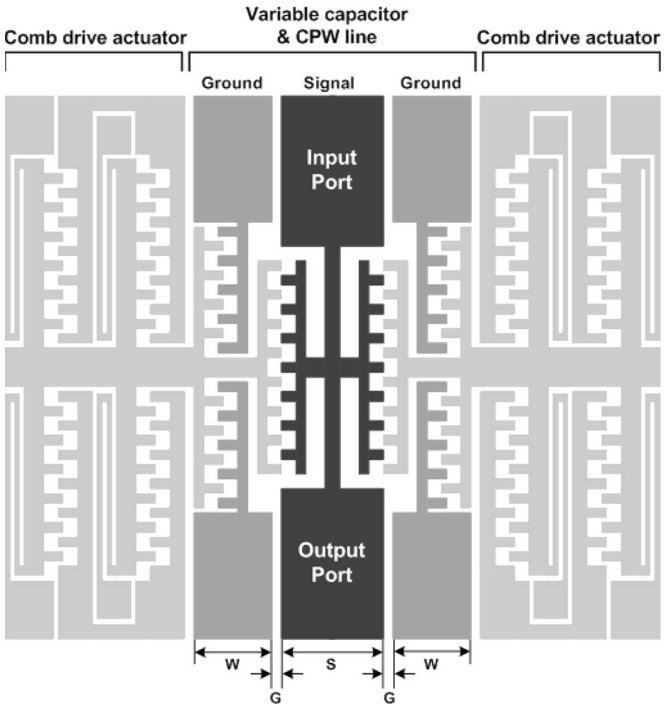

Fig. 1. Schematic diagram of the proposed non-contact-type RF MEMS switch.

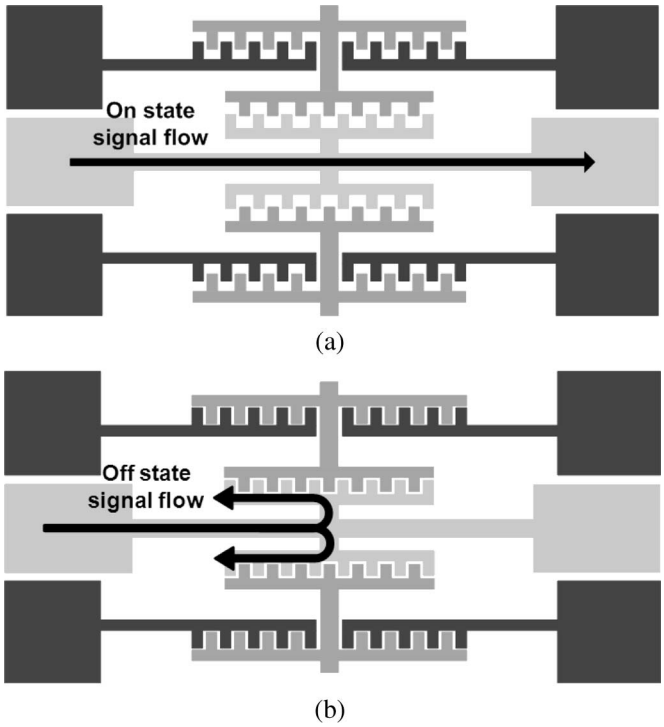

Fig. 2. ON/OFF mechanism of the proposed switch. (a) ON-state signal flow (variable capacitors are not actuated). (b) OFF-state signal flow (variable capacitors are actuated).

are totally prohibited. This prohibition is because the proposed switch is built with variable capacitor structures containing small air gaps instead of a direct or indirect contact pad. The isolated silicon stopper is designed to maintain these small gaps between combs of variable capacitor structures. The mechanical structures of the proposed switch are made of single crystal silicon (SCS). Therefore, these structures demonstrate excellent mechanical performance, high strength, no warping, and no predeformation [16].

This paper describes a non-contact-type RF MEMS switch for 24-GHz radar applications. The proposed switch is designed for use in short-range millimeter-wave radar technology that has already been implemented for various functions on automobiles such as being a component of the Intelligent Transportation System. The lumped circuit model simulations and full-wave simulations are employed to design the transmission line and the switch structure. The switch is fabricated using the selective silicon-on-insulator (SSOI) technology [17]. In this technology, horizontal dielectric layers are implanted at arbitrary depths in any desired region of a wafer, using the sacrificial bulk micromachining (SBM) process [18]–[20]. The tests are performed in 24-GHz signal switching and 10^9 cycle reliability test results with RF power. In addition, hot-switching mode power handling capacity and linearity of the fabricated switch are measured.

II. Design of Non-Contact-Type Switch

The proposed switch is a capacitive shunt type operated by the change of capacitance between the signal line and ground lines. As shown in Fig. 1, the switch consists of a coplanar waveguide (CPW) line and variable capacitors. A couple of comb-drive actuators are linked with variable capacitors for precision actuation of the capacitor structures.

The switching mechanism of the proposed switch is shown in Fig. 2. In the ON state, the variable capacitors are not actuated and the input signal passes through the CPW line, as shown in Fig. 2(a). In the OFF state, the capacitance of the actuated capacitors is changed and it prevents the signal from reaching the output port, as shown in Fig. 2(b). It is to be noted that there are small air gaps between the capacitors even in the OFF state. Therefore, the capacitors do not touch each other. Thus, the proposed switch is free from the stiction and microwelding problems of a contact-type switch. In order to have a sufficient capacitance of several hundred femtofarads in the OFF state, the comb structures are used in the variable capacitors and CPW line.

A. Transmission Line Design

The transmission line is formed from three parallel-plate wave guides running parallel to one another. This can be realized by forming 4-μm-thick evaporated copper on a released high-resistivity silicon (HRS) bridge with a large air gap. The schematic diagram of the transmission line is shown in Fig. 1. A 50-Ω transmission line impedance can be obtained by adjusting the width of the CPW signal line S, the gap width between the signal line and ground line G, and the width of the ground line W. A commercial simulation software application (Ansoft High Frequency Structure Simulator (HFSS) program) has been used for this paper. In addition, the dimensions of S, G, and W in this simulation are 166, 17, and 350 μm, respectively.

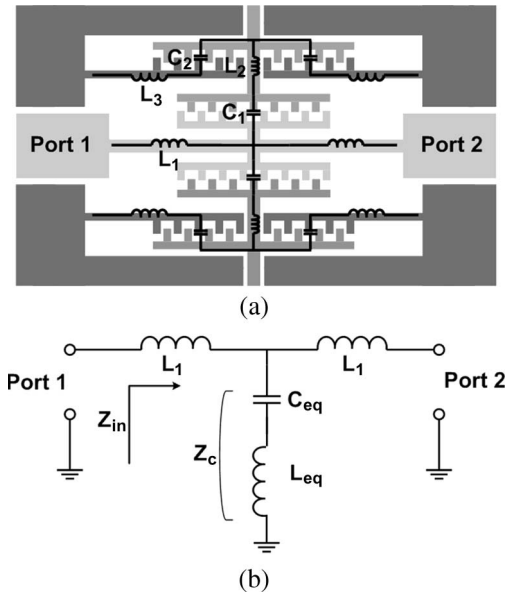

Fig. 3. Lumped circuit model of the proposed switch. (a) Inductors and capacitors of the variable capacitor structures. (b) Equivalent circuit model of the variable capacitor structures.

B. Variable Capacitor Design

The combs and bar structures of the variable capacitors are modeled with inductors and capacitors, as shown in Fig. 3(a). There are three types of inductors, namely, L_1, L_2, and L_3 and two types of capacitors, namely, C_1 and C_2. Since the structure of the switch has vertical and horizontal symmetry, there are counterparts for the labeled inductors and capacitors. The simple equivalent circuit model of the switch is shown in Fig. 3(b). The equivalent circuit model contains all of the overlapping counterparts. The equivalent inductance $L_{\rm eq}$ and the equivalent capacitance $C_{\rm eq}$ can be written as

$$L_{\rm eq} = \frac{1}{2}L_2 + \frac{1}{4}L_3 \tag{1}$$

$$C_{\rm eq} = \frac{4C_1 \cdot C_2}{C_1 + 2C_2}. \tag{2}$$

There should be a short circuit between the signal line and ground lines to obtain a high isolation in the OFF state. In addition, to obtain a low insertion loss in the ON state, the impedance, shown at port 1, should be 50 Ω when port 2 is terminated in a matched load ($Z_0 = 50\ \Omega$). Therefore, the impedance of the switch is expressed as

$$Z_{c\_\rm off} = j\omega L_{\rm eq\_off} + \frac{1}{j\omega C_{\rm eq\_off}} = 0 \tag{3}$$

$$Z_{\rm in\_on} = j\omega L_{1\_\rm on} + \frac{1}{\frac{1}{\left(j\omega L_{\rm eq\_on} + \frac{1}{j\omega C_{\rm eq\_on}}\right)} + \frac{1}{(j\omega L_{1\_\rm on} + Z_0)}} = Z_0 \tag{4}$$

where the OFF-state impedance $Z_{c\_\rm off}$ contains an OFF-state capacitance $C_{\rm eq\_off}$ and the OFF-state inductance $L_{\rm eq\_off}$. The ON-state impedance $Z_{\rm in\_on}$ is shown at port 1. This impedance consists of ON-state inductances, namely, $L_{1\_\rm on}$ and $L_{\rm eq\_on}$, the ON-state capacitance $C_{\rm eq\_on}$, and the impedance of the matched load Z_0. There are several combinations of inductances and capacitances that satisfy (3) and (4) at 24 GHz. One of the combinations of inductances and capacitances is presented in Table II. These values are determined using the Agilent Advanced Design System program.

TABLE II
INDUCTANCE AND CAPACITANCE COMBINATION FOR 24-GHz SWITCH

	On state	Off state
L_1	0.19 nH	0.19 nH
L_2	0.22 nH	0.19 nH
L_3	0.19 nH	0.19 nH
C_1	43.1 fF	285 fF
C_2	130 fF	158 fF

The physical dimensions of the inductors and capacitors are determined by a full-wave simulation using the HFSS program. The 3-D model for the full-wave simulation and the detailed dimensions of the variable capacitors are shown in Fig. 4. The actuation distance is designed to be 25 μm. The inductors and capacitors are built up of 4-μm-thick evaporated copper on released HRS structures. The inductor L_1 has a width of 40 μm, a thickness of 4 μm, and a length of approximately 360 μm. The inductor L_2 has the same cross-sectional area but different lengths of approximately 375 μm in the OFF state and 400 μm in the ON state. It is more difficult to find the dimensions of the inductor L_3 than the other inductors because it is in the same space as C_2. Therefore, the dimensions of C_2 are adjusted and the inductance of L_3, approximately 0.19 nH, is calculated from the resonant frequency of C_2 and L_3 [21]. While the capacitance of C_2 is larger than that of C_1, the variation in the capacitance C_2 is smaller than that of C_1. The width and the pitch of the comb fingers of C_1 are 2 and 7 μm, respectively, and the width and the pitch of the comb fingers of C_2 are 2 and 10 μm, respectively. Since the 4-μm-thick copper evaporates on the top surface of the etched silicon structure that is normally in the ON state, the space of the nearest comb fingers of C_2 is designed to be larger than 2 μm to prevent contact between the capacitors.

The lumped circuit model simulation and full-wave simulation results of the designed switch are shown in Fig. 5. In the ON-state simulation results, the insertion loss values are 0.1 dB in the circuit model simulation and 0.27 dB in the full-wave simulation. The isolation values of the circuit model simulation results and the full-wave simulation results are 49 and 47 dB, respectively, at 24 GHz, as shown in Fig. 5. The full-wave simulation properties, near 24 GHz, are similar to the calculated data of the lumped circuit model. The insertion loss is larger than the calculated result because the lumped circuit model does not consider the resistance.

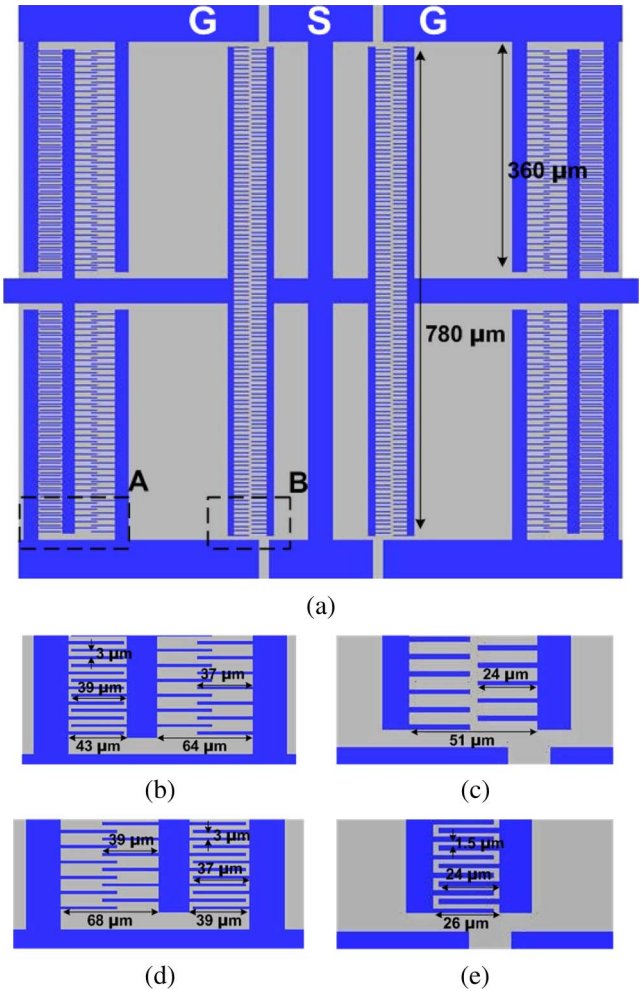

Fig. 4. Three-dimensional model and the determined dimensions of variable capacitor structures for the full-wave simulation. (a) Full-wave simulation model of the switch, and detailed dimensions of (b) area A in the ON state, (c) area B in the ON state, (d) area A in the OFF state, and (e) area B in the OFF state.

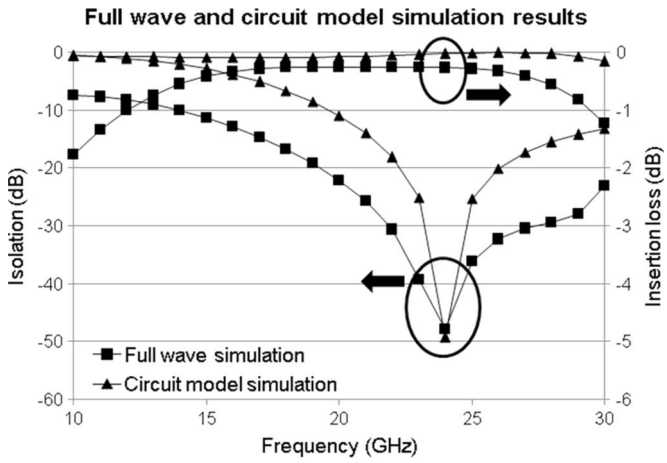

Fig. 5. Lumped circuit model simulation and full-wave simulation results of the designed switch.

C. Actuator Design

In this paper, we use the comb-drive actuator with folded springs for precision control of the switch displacement. The variable capacitor is extended from the mass of the actuator. The relationship between the driving voltage and the displacement in the comb-drive actuator can be expressed as [22]

$$F_k = kd = \frac{2Etw^3}{L^3}d \tag{5}$$

$$F_e = \frac{\varepsilon tNV^2}{g} \tag{6}$$

$$F_k = F_e \rightarrow V = \sqrt{\frac{2Ew^3d}{L^3}\frac{g}{\varepsilon N}} \tag{7}$$

where F_k is a restoring force, k is the mechanical spring constant, $E = 168.9$ GP is the Young's modulus, t is the spring and structure thickness, w is the spring width, L is the spring length, d is the stroke of the actuator, F_e is an electrostatic force, $\varepsilon = 8.854 \times 10^{-12}$ F/m is the permittivity, N is the number of combs, V is the switch control voltage, and g is the gap between moving combs and stationary combs. The schematic diagram of the mechanical spring is shown in Fig. 6. The target actuation stroke is 25 μm as described in the variable capacitor design section. The spring length, the spring width, the structure thickness, and the gap between the combs are 650, 5, 40, and 2.1 μm, respectively, due to the fabrication issues. The control voltage is set below 30 V, because the RF measurement system cannot withstand high voltage. The detailed dimensions of the comb-drive actuator, considering design factor and constraint, are summarized in Table III. In this case, the total mass of the designed switch structure is 45.432 μg, and the total spring constant of mechanical springs is 6.150 N/m. The mechanical resonant frequency of the designed switch is 1.851 kHz.

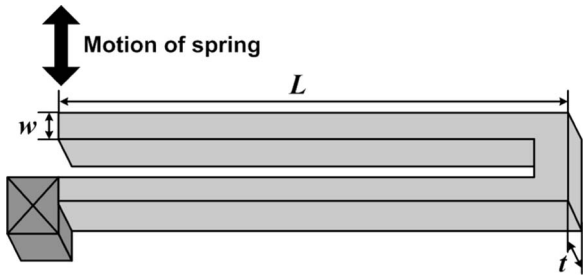

Fig. 6. Schematic diagram of the mechanical spring.

TABLE III
DETAILED DIMENSIONS OF THE COMB-DRIVE ACTUATOR

		Designed dimensions
Comb finger	Number	1000
	Thickness	40 μm
	Length	27 μm
	Gap	2.1 μm
Folded beam spring	Width	5 μm
	Thickness	40 μm
	Length	650 μm

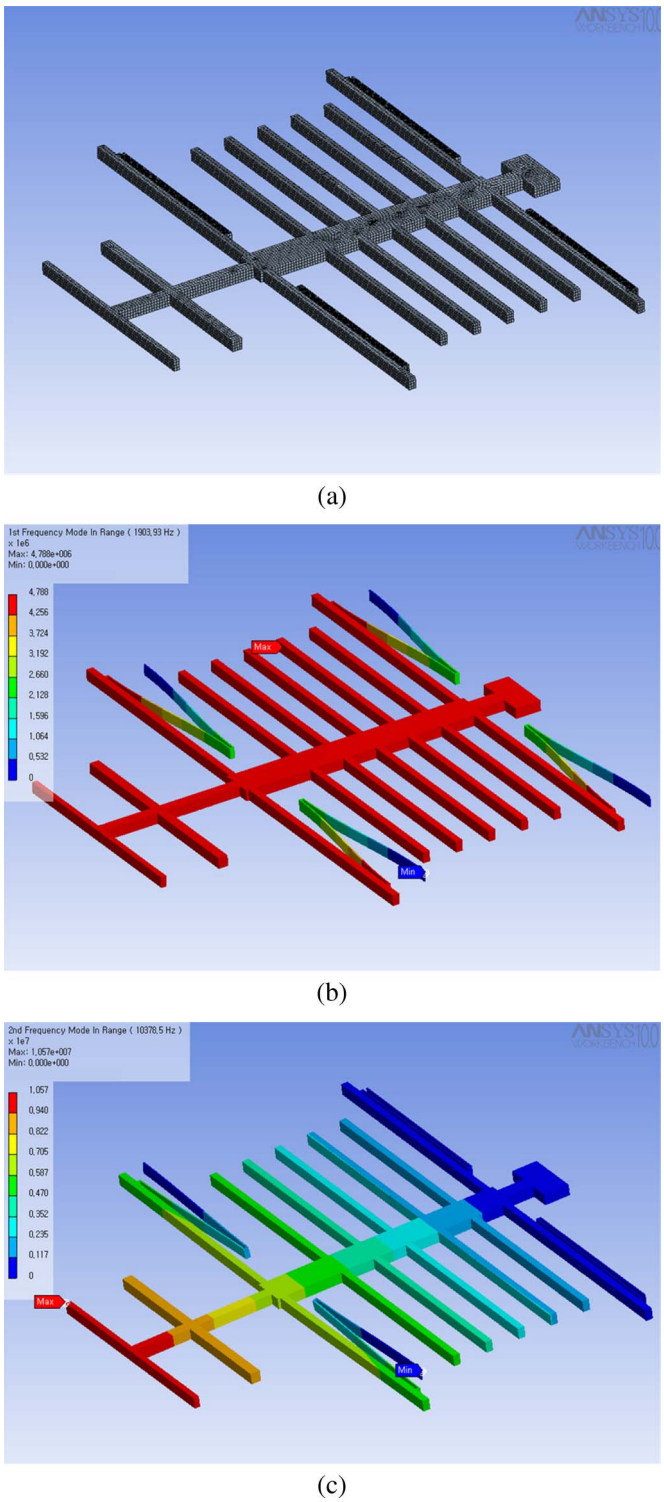

Fig. 7. Modal analysis of the proposed switch structure. (a) FEM model of the proposed switch structure, (b) rectilinear motion of the switch at the prime mode, and (c) tilting motion of the switch at the second mode.

In order to analyze the actuation motion of the designed switch structure, finite element method (FEM) modeling on the switch structure is performed using ANSYS v10.0. Quadrilateral elements have been used for area meshing. The simulation model and the simulation results are shown in Fig. 7. The prime mode represents the expected rectilinear motion at 1.903 kHz, as shown in Fig. 7(b). The second mode appears at 10.378 kHz with a tilting motion, and it is separated by five times the prime mode frequency. This large difference between the prime mode and the second mode guarantees a stable mechanical actuation mode without interference phenomenon.

III. Fabrication Process

The proposed switch design requires a large and precise mechanical motion and an air bridge with a large air gap for the low-loss CPW line. However, this is extremely difficult for conventional polysilicon or SCS processes, including the silicon-on-insulator (SOI) technology, because the air gap of the low-loss CPW line is limited to several micrometers and the inevitable residual stress and the footing phenomenon can cause a structural fracture and degradation in the SOI process [17], [23]. Mechanical stress is induced by the disparity of the silicon and silicon dioxide thermal expansion coefficient. The silicon structure, fabricated by the SOI process, has a 35-MPa tensile stress [17]. This large stress, in turn, causes the released large structures to break and bend or twist. In addition, the deep silicon reactive ion etching (RIE) on the SOI wafer leads to the well-known footing phenomenon [23]–[26]. Several companies developed the SOI kit to solve the aforementioned problems. One such company, Surface Technology Systems Limited (STS, UK), provides advanced silicon etching technology.[1] However, there is a significant difference of the trench opening size between the mechanical spring and the comb-drive actuator part in a large displacement actuator. In this case, it is difficult to remove completely the footing phenomenon. To demonstrate the mentioned problems using a conventional SOI process, the designed switch is fabricated on a SOI wafer. The SOI process is composed of single photolithography, deep silicon RIE, and hydrofluoric release processes [27]. In this fabrication, the SOI kit is not used and the switch structure is fabricated on a 450-μm (100) SOI wafer. The device layer thickness of the SOI wafer is 50 μm, and the oxide layer thickness is 2 μm. The scanning electron microscope (SEM) photographs of the fabricated switch structure are shown in Fig. 8. The spring part of the switch structure is broken by a residual stress, as shown in Fig. 8(a). In this switch design, the residual stress of the SOI wafer has enormous influence on the large released structure, which is used for large displacement. In Fig. 8(b), the footing phenomenon is observed in the spring part, which has a relatively large etch area. In the end, these problems degrade the performance of the switch and the process yield of the switch fabrication. The large air gap for the low-loss CPW line can be fabricated using the SOI wafer with preprocessed handle layer, which is similar to the silicon-on-glass process [28], [29]. However, the disadvantage of this method is the difficult wafer preparation, which requires the handle wafer etch process and the precision wafer bonding process.

The SSOI process, based on the SBM process, is used for solving the problems of conventional polysilicon or SCS processes [16]–[19]. The SSOI process is comprised of two times the SBM process and a gap filling process. This process

[1] [Online]. Available: http://www.stsystems.com/.

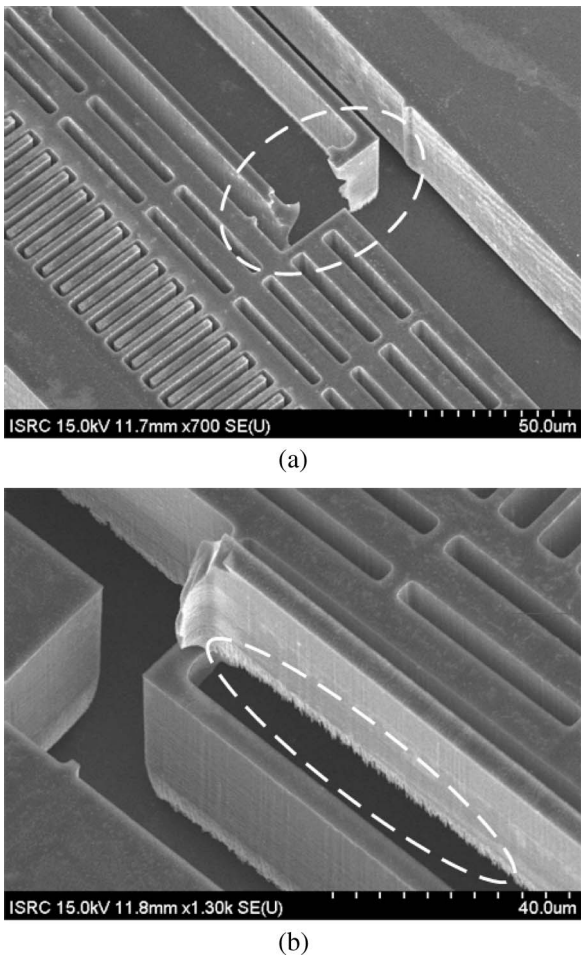

Fig. 8. Fabrication results of the switch structure using the SOI process. This was done to show the inherent problems of the SOI process. That is, the footing-induced problems and residual stress-induced problems are inevitable. (a) SEM photograph of the mechanical spring part broken by the residual stress. (b) SEM photograph showing the footing phenomenon of the bottom surface of the spring part.

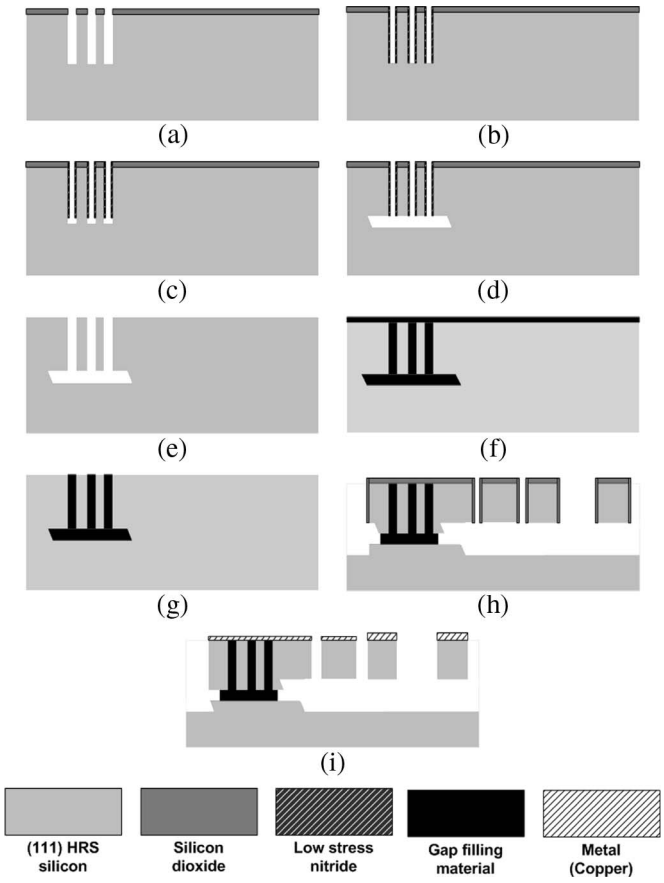

Fig. 9. Process flow of the non-contact-type switch. (a) Trench patterning and silicon deep RIE, (b) sidewall passivation, (c) silicon RIE, (d) release of anchor part in alkaline etchant, (e) etch mask removal, (f) gap refilling, (g) top insulation layer etch, (h) second SBM process, and (i) etch mask removal and metal deposited.

is suitable for electrically isolating the released high-aspect-ratio SCS MEMS structures with almost no residual stress, no footing phenomenon, and a large sacrificial gap. The fabrication process is shown in Fig. 9. The fabrication process starts with p-type float zone $\langle 111 \rangle$ HRS $(10^3 - 10^5\ \Omega \cdot \mathrm{cm})$. First, a plasma-enhanced chemical vapor deposition tetraethylorthosilicate (TEOS) oxide layer is deposited as a hard mask for deep silicon RIE and then subsequently patterned. Then, photolithography is performed to define the trench pattern of the electrode to be released. Next, a deep silicon RIE process is used to define the depth of the isolation layer, as shown in Fig. 9(a). Then, for protecting the structure sidewalls in alkaline etching, low-stress nitride is deposited, as shown in Fig. 9(b). The sidewall passivation films are then anisotropically etched using RIE to expose bare silicon at the bottom of the etched trenches. Then, the silicon wafer is vertically etched again to define the sacrificial gap for the electrode area, as shown in Fig. 9(c). After this etching, the wafer is dipped into an aqueous alkaline solution to release the electrode areas, as shown in Fig. 9(d). After the silicon wet etching process, the mask and passivation films are removed. Up to this step, the first SBM process is completed for the isolated anchor release. Then, the gap is filled with 3000 Å of thermal oxide, 2000 Å of low-stress nitride, and 4 μm of low-pressure chemical vapor deposition polysilicon films. The oxide and nitride films work as an insulation between the electrode and the substrate and as a protective layer for polysilicon films during the wet etch of the second SBM process. Then, the polysilicon/nitride/oxide films on the top surface are removed and the desired devices are fabricated using the second SBM process, as shown in Fig. 9(g) and (h). Finally, the etch masks are removed and the metal layer is deposited, as shown in Fig. 9(i). In the metal deposition step, a 4-μm-thick copper is evaporated in the variable capacitors and CPW line for the RF signal flow. Thin copper is evaporated in the comb-drive actuator areas. The metal thickness difference is due to preventing the electrical short problem between the moving and stationary combs of the comb-drive actuators.

The SEM photographs of the fabricated switch are shown in Fig. 10. As shown in Fig. 10(a), for this relatively large size of 4 mm $\times$ 5 mm, there is no noticeable structure bending or twisting. The magnified view of the variable capacitor structure and CPW line with the signal flow indication is shown in Fig. 10(b). The comb-drive actuator and the isolated silicon stopper structure are shown in Fig. 10(c). The isolated silicon stopper structure is utilized for preventing the contact that may

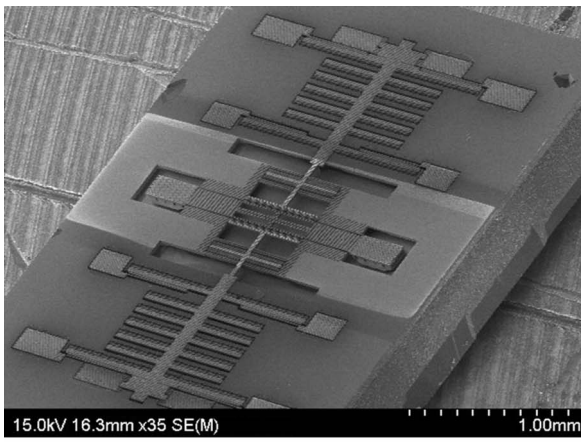

(a)

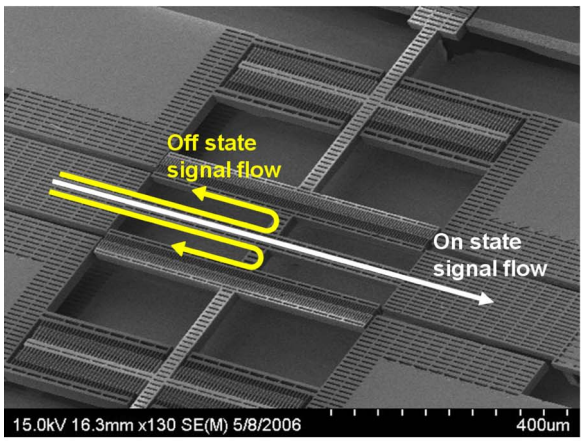

(b)

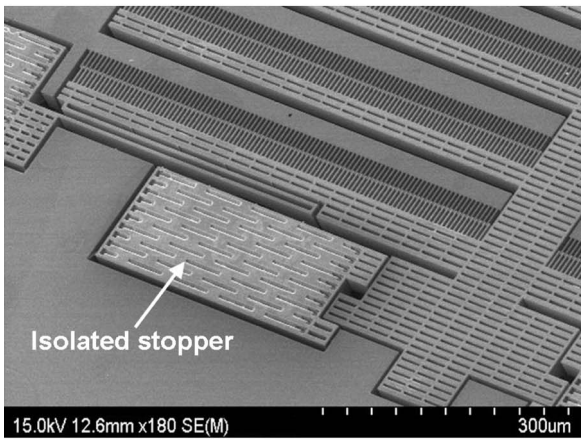

(c)

Fig. 10. SEM photographs of the fabricated switch. (a) Complete view of the fabricated switch, (b) the magnified view of the variable capacitor structures, and (c) the magnified view of the comb-drive actuator and isolated silicon stopper structure.

occur in the variable capacitor structure. Although there can still be tiny contact between the auxiliary part of the switch structure and the isolated stopper, the stiction problem is not generated because of the high mechanical strength of the silicon structure [16], [30]. This small silicon stopper has been used in several MEMS devices [31], [32]. The length of the CPW line is 1.5 mm. The thickness of the structure is 35 μm, and the sacrificial gap of the moving structure and the air gap of the

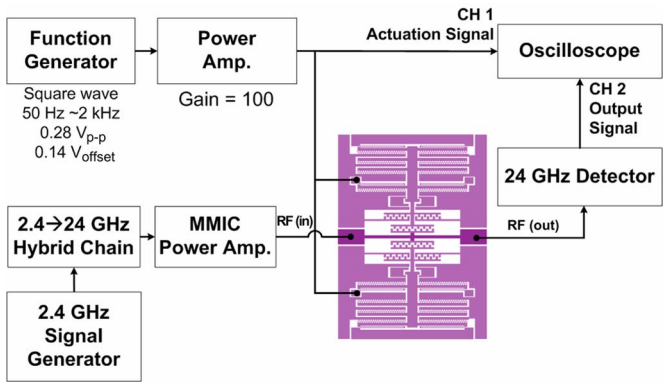

Fig. 11. Measurement setup for the switching time.

silicon bridge are 30 μm. The minimum gap of the comb drive is 2.1 μm.

IV. Measurement Results

A. Mechanical Characteristics

In the direct-current (dc) driving mode, the actuation stroke of the fabricated switch was 25 μm at a 25-V driving voltage. The frequency response of the fabricated switch was measured using the Agilent 35670A spectrum analyzer. The measured mechanical resonant frequency of the fabricated switch was 1.501 kHz which was lower than the simulation results. The two major reasons for the difference were the changes of the spring width and the structure thickness. In the simulation, the spring width was 5 μm and the structure thickness was 40 μm. However, in the fabrication results, the spring width was changed to 4.4 μm due to the undercut of the deep silicon RIE step. In addition, in consequence of the fabrication process error, the structure thickness was changed to 35 μm.

The switching time was measured using a measurement setup as shown in Fig. 11. As a switch actuation signal, a square wave, with a frequency of 50 Hz and a voltage magnitude of 28 V, was supplied by the Agilent 33120A function generator and the TREK model 603 power amplifier. An RF input signal of 24-GHz continuous RF power from millimeter-wave monolithic integrated circuit (MMIC) chip power amplifier was applied to the fabricated switch. The MMIC power amplifier was made using SiGe heterojunction bipolar transistor (HBT), and the emitter sizes of SiGe HBT were 320 and 160 μm^2. The gain of the MMIC power amplifier was 12 dB at 24 GHz. The maximum output power of the MMIC power amplifier was 21 dBm at 24 GHz. The power of the input signal was 18 mW, and that was the maximum power available in this measurement setup. The modulated RF envelope that resulted from the switch actuation and actuation signal was measured by Agilent 54624A oscilloscope.

The measurement results of the switching time are shown in Fig. 12. The measured envelope of the RF output signal is the upper trace that is modulated by the actuation signal as shown in the lower trace. The measured switching times are 300 μs for the transition from the OFF to the ON state and 200 μs for the transition from the ON to the OFF state. In the ON state,

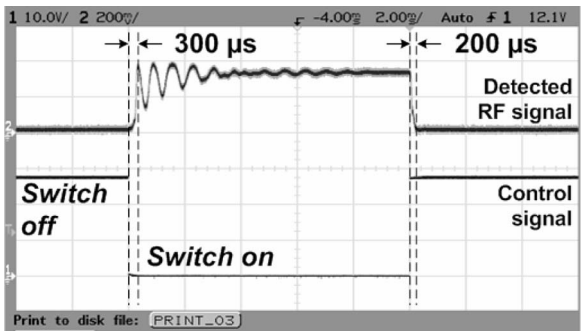

Fig. 12. Measurement results of the switching time.

8 ms is the time taken for the oscillating motion of the actuator to vanish.

The reliability of the fabricated switch was tested in an ambient atmosphere. The measurement setup for the reliability test was the same as that of the switching time measurement. The switch could be operated at a maximum control signal frequency of 2 kHz. Therefore, as a switch actuation signal, a square wave with a frequency of 2 kHz and a voltage magnitude of 28 V was applied. The RF input power was 18 mW, as used in the switching time measurement. Even after 10^9 continuous cycles of mechanical actuation, mechanical failures, including the stiction problem and deformation of the structure, were not detected. In addition, no RF performance degradation was observed.

B. RF Characteristics

The RF characteristics of the fabricated non-contact-type switch were measured using an HP 8510 XF vector network analyzer with tungsten-tip 250-μm-pitch ground-signal-ground coplanar probes (GGB Industries Inc. Picoprobe). The system was calibrated using a standard short-open-load-through calibration technique. The calibration substrate was GGB Industries INC. CS-5 calibration substrate.[2] External electrical control signals were applied on the fabricated switch for actuation. The s-parameters of the input and output ports were extracted using a network analyzer. The insertion loss and isolation of the switch were characterized by S21 through the input and output ports in the ON and OFF states of the switch.

The RF characteristic measurement results for the fabricated switch are shown in Fig. 13. To compare simulation results and measurement results, the full-wave simulation results are drawn in the same graph. In the ON state, the insertion loss is 1.43 dB at 24 GHz. However, this result includes the signal loss of the long CPW lines. The insertion loss, the signal loss only in the variable capacitor structure, is 0.29 dB. To determine the signal loss in the CPW line, the CPW line without variable capacitor structures was fabricated in the first place. Then, the signal loss in the CPW line was measured. The length of the CPW line, which has been used for the signal loss measurement, is equal to the length of the CPW line in the switch structure. In the OFF state, the peak is not exactly at 24 GHz, but the isolation is 30.1 dB as shown in Fig. 13(b).

[2][Online]. Available: http://www.picoprobe.com/.

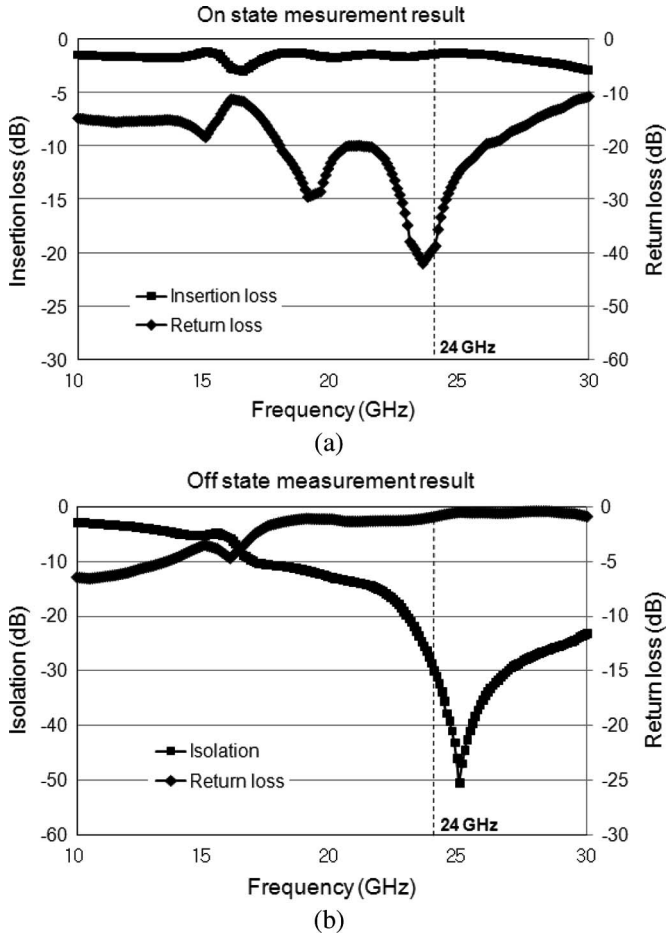

Fig. 13. Measured RF characteristics of the fabricated non-contact-type switch. (a) Measured insertion loss in the ON state and (b) measured isolation in the OFF state.

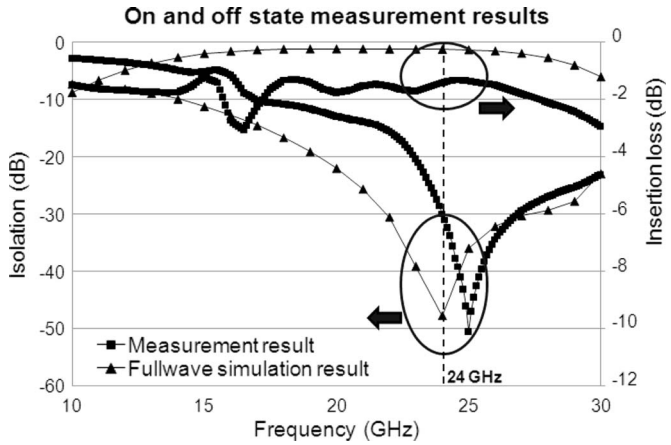

Fig. 14. Comparison of simulation results of the designed switch and measurement results of the fabricated switch.

The maximum isolation value is 50.5 dB at 25 GHz. From 23.5 to 29 GHz, the isolation is better than 25 dB.

The full-wave simulation results and measurement results were compared as shown in Fig. 14. The output characteristics of the fabricated switch matched similarly with the full-wave simulation results. However, the peak of isolation was not exactly at 24 GHz in the OFF-state measurement results, and the measured insertion loss was larger than the simulation results.

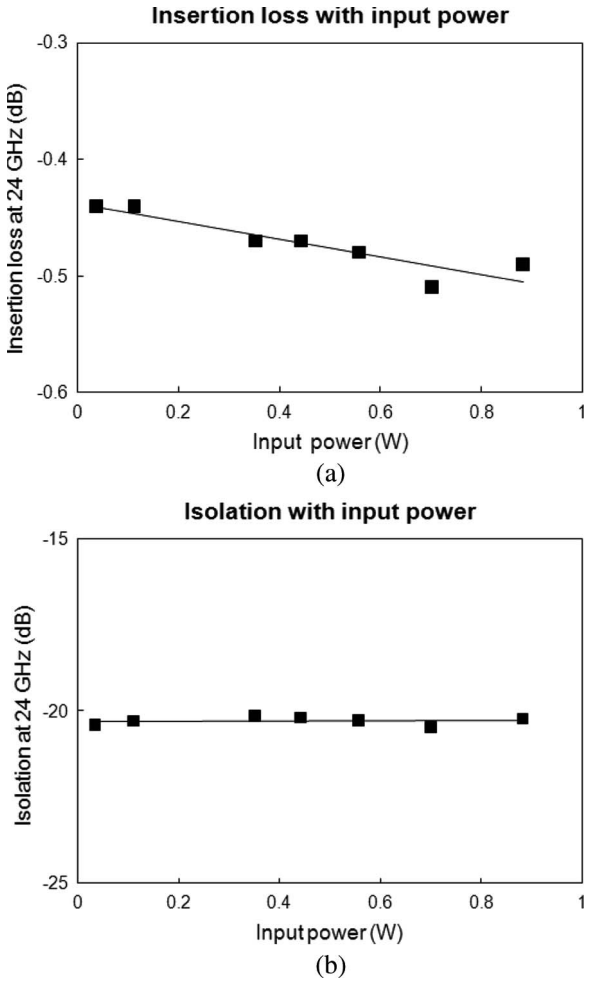

Fig. 15. Measurement results of the insertion loss and isolation with input power. (a) Measured insertion loss with input power at 24 GHz and (b) measured isolation with input power at 24 GHz.

The discrepancy between the measurement results and simulation results was caused by the fabrication process uncertainties in the photolithography and deep silicon RIE steps. In addition, an unwanted peak was measured in the ON- and OFF-state measurement results because the discontinuity in the full-wave simulation was not considered.

The power handling capacity and linearity of the fabricated switch is measured in hot-switching mode. Hot-switching mode power handling capacity and linearity properties were measured simultaneously, and the limit of the input RF power level was 0.9 W in our experimental setup. The ON-state measurement was performed by applying input RF power and calculating the insertion loss from the measured output RF power. The measured insertion loss did not contain the CPW line loss. The OFF-state measurement was performed by actuating the switch with a dc voltage of 28 V without reducing the input RF power. Then, the isolation was calculated from the corresponding measured output power. The measurement results are summarized in Fig. 15. The insertion loss was slightly increased when increasing the input RF power, but the isolation was constant up to 0.9 W. A small nonlinearity in the ON state was observed. In addition, latching or self-actuation was not detected up to 0.9 W. In order to measure the self-actuation power level, a dc bias was applied between the RF signal line and ground line directly using a voltage source. Self-actuation was observed at an applied power of 27 and 34 V, respectively. The root-mean-square potentials of 27 and 34 V were obtained from 29 and 46 W of RF power.

V. Conclusion

In this paper, we described our development of a non-contact-type RF MEMS switch for 24-GHz radar applications. This switch is a capacitive shunt type operated by the change in capacitance between the signal line and ground lines. The switching mechanism is unique due to the small air gaps between the capacitors even in the OFF state. Therefore, the normal problems of the contact switch do not occur in this switch. To realize the large and precise mechanical motion of the switch, the SSOI process is used for switch fabrication. The actuation voltage of the fabricated switch is 25 V, and the actuation stroke is 25 μm. This large motion is feasible by using bulk silicon. The same design fabricated by the more conventional SOI process breaks due to residual stress. The measured switching times are 8 ms from the OFF to the ON state. However, the first peak appeared within 300 μs from the drop of the control voltage. For the transition from the ON to the OFF state, about 200 μs was taken. The RF characteristics of the fabricated non-contact-type switch have been measured using a vector network analyzer. In the ON state, the insertion loss is 1.43 dB at 24 GHz. However, the extract signal loss only in the variable capacitor structure is 0.29 dB. In the OFF state, because of the fabrication process uncertainties, the peak is not exactly at 24 GHz, but the isolation is 30.1 dB. The isolation is 25 dB or better for the range from 23.5 to 29 GHz. The switch could withstand over 0.9 W of 24-GHz RF power under hot-switching condition with high linearity. By a self-actuation test, it could be inferred that self-actuation would not be detected in an RF power below 29 W. In the reliability test with RF power, mechanical failures are not detected after 10^9 cycle actuation. In addition, the entire structure of the switch has been fabricated using high-resistivity SCS. Therefore, the fabricated switch demonstrated excellent mechanical performance and properties.

Acknowledgment

The authors would like to thank Dr. S. Han of MANDO Corporation and Dr. I. Lee, Dr. J. Lee, and Dr. I. Moon of Hyundai Motor Corporation for their help in automotive applications and testing. The authors would also like to thank Prof. J. No and Prof. S. Nam of Seoul National University for their advice throughout the project.

References

[1] C. T.-C. Nguyen, L. P. B. Katehi, and G. M. Rebeiz, "Micromachined devices for wireless communications (invited)," *Proc. IEEE*, vol. 86, no. 8, pp. 1756–1768, Aug. 1998.

[2] G. M. Rebeiz and J. B. Muldavin, "RF MEMS switches and switch circuits," *IEEE Microw. Mag.*, vol. 2, no. 4, pp. 59–71, Dec. 2001.

[3] H. A. C. Tilmans, "MEMS components for wireless communications (invited paper)," in *Proc. EUROSENSORS XVI*, Sep. 2003, pp. 1–34.

[4] J. J. Yao, "RF MEMS from a device perspective," *J. Micromech. Microeng.*, vol. 10, no. 4, pp. R9–R38, Dec. 2000.
[5] K. E. Petersen, "Micromechanical membrane switches on silicon," *IBM J. Res. Develop.*, vol. 23, no. 4, pp. 376–385, Jul. 1979.
[6] W. P. Taylor and M. G. Allen, "Integrated magnetic microrelays: Normally open, normally closed, and multi-pole devices," in *Proc. Tech. Dig., Int. Conf. Solid-State Sens. Actuators (TRANSDUCERS)*, Jun. 1997, pp. 1149–1152.
[7] H. A. C. Tilmans, E. Fullin, H. Ziad, M. D. J. Van de Peer, J. Kesters, E. Van Geffen, J. Bergqvist, M. Pantus, E. Beyne, K. Baert, and F. Naso, "A fully-packaged electromagnetic microrelay," in *Proc. Tech. Dig., 12th IEEE Int. Conf. Micro Electro Mech. Syst.*, Jan. 1999, pp. 25–30.
[8] Z. J. Yao, S. Chen, S. Eshelman, D. Denniston, and C. Goldsmith, "Micromachined low-loss microwave switches," *J. Microelectromech. Syst.*, vol. 8, no. 2, pp. 129–134, Jun. 1999.
[9] C. Bozler, R. Drangmeister, S. Duffy, M. Gouker, J. Knecht, L. Kushner, R. Parr, S. Rabe, and L. Travis, "MEMS microswitch arrays for reconfigurable distributed microwave components," in *Tech. Dig., IEEE Int. Microw. Symp.*, Jun. 2000, pp. 153–156.
[10] J. B. Muldavin and G. M. Rebeiz, "All-metal high-isolation series and series/shunt MEMS switches," *IEEE Microw. Wireless Compon. Lett.*, vol. 11, no. 9, pp. 373–375, Sep. 2001.
[11] J. Oberhammer and G. Stemme, "Low-voltage high isolation DC-to-RF MEMS switch based on an s-shaped film actuator," *IEEE Trans. Electron Devices*, vol. 51, no. 1, pp. 149–155, Jan. 2004.
[12] J.-M. Kim, J.-H. Park, C.-W. Baek, and Y.-K. Kim, "The SiOG-based single-crystalline silicon (SCS) RF MEMS switch with uniform characteristics," *J. Microelectromech. Syst.*, vol. 13, no. 6, pp. 1036–1042, Dec. 2004.
[13] H.-C. Lee, J.-Y. Park, and J.-U. Bu, "Piezoelectrically actuated RF MEMS DC contact switches with low voltage operation," *IEEE Microw. Wireless Compon. Lett.*, vol. 15, no. 4, pp. 202–204, Apr. 2005.
[14] I.-J. Cho, T. Song, S.-H. Baek, and E. Yoon, "A low-voltage and low-power RF MEMS series and shunt switches actuated by combination of electromagnetic and electrostatic forces," *IEEE Trans. Microw. Theory Tech.*, vol. 53, no. 7, pp. 2450–2457, Jul. 2005.
[15] E. J. J. Kruglick and K. S. J. Pister, "Lateral MEMS microcontact considerations," *J. Microelectromech. Syst.*, vol. 8, no. 3, pp. 264–271, Sep. 1999.
[16] M. Tang, A. Agarwal, J. Li, Q. X. Zhang, P. Win, J. M. Huang, and A. Q. Liu, "An approach of lateral RF MEMS switch for high performance," in *Tech. Dig., Design, Test, Integr. Packag. MEMS/MOEMS*, May 2003, pp. 99–102.
[17] S. J. Park, D. H. Kwak, H. H. Ko, T. Y. Song, and D. I. Cho, "Selective silicon-on-insulator (SOI) implant: A new micromachining method without footing and residual stress," *J. Micromech. Microeng.*, vol. 15, no. 9, pp. 1607–1613, Sep. 2005.
[18] S. Lee, S. Park, and D. Cho, "A new micromachining technology using (111) silicon," in *Proc. Tech. Dig., Microprocess Nanotechnol. Conf.*, Jul. 1998, pp. 174–175.
[19] S. Lee, S. Park, and D. Cho, "The surface/bulk micromachining (SBM) process: A new method for fabricating released MEMS in single crystal silicon," *J. Microelectromech. Syst.*, vol. 8, no. 4, pp. 409–416, Dec. 1999.
[20] S. Lee, S. Park, J. Kim, S. Lee, and D. Cho, "Surface/bulk micromachined single-crystalline silicon micro-gyroscope," *J. Microelectromech. Syst.*, vol. 9, no. 4, pp. 557–567, Dec. 2000.
[21] C. P. Yue and S. S. Wong, "Physical modeling of spiral inductors on silicon," *IEEE Trans. Electron Devices*, vol. 47, no. 3, pp. 560–568, Mar. 2000.
[22] R. Legtenberg, A. W. Groeneveld, and M. Elwenspoek, "Comb-drive actuators for large displacements," *J. Micromech. Microeng.*, vol. 6, no. 3, pp. 320–329, Sep. 1996.
[23] J. Kim, S. Park, D. Kwak, H. Ko, W. Carr, J. Buss, and D. Cho, "Robust SOI process without footing and its application to ultra high-performance microgyroscopes," in *Tech. Dig., Int. Conf. Solid-State Sens. Actuators (TRANSDUCERS)*, Jun. 2003, pp. 1691–1694.
[24] J. Arnold and H. Sawin, "Charging of pattern features during plasma etching," *J. Appl. Phys.*, vol. 70, no. 10, pp. 5314–5317, Nov. 1991.
[25] G. Hwang and K. Giapis, "On the origin of the notching effect during etching in uniform high density plasmas," *J. Vac. Sci. Technol. B, Microelectron. Process. Phenom.*, vol. 15, no. 1, pp. 70–87, Jan. 1997.
[26] A. Ayón, K. Ishihara, R. Braff, H. Sawin, and M. Schmidt, "Microfabrication and testing of suspended structures compatible with silicon-on-insulator technology," *J. Vac. Sci. Technol. B, Microelectron. Process. Phenom.*, vol. 17, no. 4, pp. 1589–1593, Jul. 1999.
[27] B. Diem, M. T. Delaye, F. Michel, S. Renard, and G. Delapoerre, "SOI (SIMOX) as a substrate for surface micromachining of single crystalline silicon sensors and actuators," in *Tech. Dig., Int. Conf. Solid-State Sens. Actuators (TRANSDUCERS)*, Jun. 1993, pp. 233–236.
[28] M. Chabloz, J. Jiao, Y. Yosida, T. Matsuura, and K. Tsutsumi, "A method to evade microloading effect in deep reactive ion etching for anodically bonded glass-silicon structures," in *Tech. Dig., 13th IEEE Int. Conf. Micro Electro Mech. Syst.*, Jan. 2000, pp. 283–287.
[29] J. Chae, H. Kulah, and K. Najafi, "A hybrid Silicon-On-Glass (SOG) lateral micro-accelerometer with CMOS readout circuitry," in *Tech. Dig. 15th IEEE Int. Conf. Micro Electro Mech. Syst.*, Jan. 2002, pp. 623–625.
[30] K. E. Petersen, "Silicon as a mechanical material," *Proc. IEEE*, vol. 70, no. 5, pp. 420–457, May 1982.
[31] M. Mita, M. Arai, S. Tensaka, D. Kobayashi, P. Basset, A. Kaiser, P. Masquelier, L. Buchaillot, D. Collard, and H. Fujita, "Electrostatic impact-drive microactuator," in *Tech. Dig. 14th IEEE Int. Conf. Micro Electro Mech. Syst.*, Jan. 2001, pp. 590–593.
[32] R. Abdolvand, B. V. Amini, and F. Ayazi, "Sub-micro-gravity in-plane accelerometers with reduced capacitive gaps and extra seismic mass," *J. Microelectromech. Syst.*, vol. 16, no. 5, pp. 1036–1043, Oct. 2007.

Jaehong Park was born in Korea in 1978. He received the B.S. and M.S. degrees in electrical engineering and computer science from Seoul National University, Seoul, Korea, in 2002 and 2004, respectively. He is currently working toward the Ph.D. degree in the School of Electrical Engineering and Computer Science, Seoul National University.

His research interests include design, optimization, and fabrication of microactuators and microsensors.

Eun Sub Shim was born in Korea in 1978. He received the B.S. and M.S. degrees in electrical engineering from Yonsei University, Seoul, Korea, in 2001 and 2003, respectively. He is currently working toward the Ph.D. degree in electrical engineering in the School of Electrical Engineering and Computer Science, Seoul National University, Seoul.

His current research interests include design, fabrication, and applications of various MEMS sensors.

Wooyeol Choi was born in Korea in 1979. He received the B.S. degree from Yonsei University, Seoul, Korea, in 2001, and the M.S. degree from Seoul National University, Seoul, in 2003, both in electrical engineering. He is currently working toward the Ph.D. degree in electrical engineering in the School of Electrical Engineering and Computer Science, Seoul National University.

Since 2002, he has been with the Three-Dimensional Millimeter-Wave Integrated Systems (C3DM) Group, Seoul National University. His research interests include the design of millimeter-wave integrated circuits and systems using GaAs and Si devices.

Youngmin Kim was born in Masan, Korea, in 1979. He received the B.S. degree in electronic engineering from Sung Kyun Kwan University, Seoul, Korea, in 2001, and the M.S. degree in electrical engineering from Seoul National University, Seoul, in 2005. He is currently working toward the Ph.D. degree in the School of Electrical Engineering and Computer Science, Seoul National University.

His current research interests include the design of MMICs for millimeter-wave systems using GaAs and Si devices and their system integration.

Youngwoo Kwon (S'90–M'94–SM'04) was born in Korea in 1965. He received the B.S. degree in electronics engineering from Seoul National University, Seoul, Korea, in 1988, and the M.S. and Ph.D. degrees in electrical engineering from the University of Michigan, Ann Arbor, in 1990 and 1994, respectively.

From 1994 to 1996, he was with the Rockwell Science Center as a Member of Technical Staff and was involved in the development of millimeter-wave monolithic integrated circuits. In 1996, he joined the School of Electrical Engineering and Computer Science, Seoul National University, where he is currently a Professor. Over the past years, he has directed a number of RF research projects funded by the Korean government and U.S. companies. He has authored or coauthored more than 150 technical papers in internationally renowned journals and conference proceedings. He is the holder of more than 20 patents on RF MEMS and power amplifier technology. He is also a co-inventor of the switchless stage-bypass power amplifier architecture called "CoolPAMTM" and co-founded Wavics, a power amplifier design company, which is now fully owned by Avago Technologies.

Dr. Kwon is an Associate Editor for the IEEE TRANSACTIONS ON MICROWAVE THEORY AND TECHNIQUES. He has also served as technical program committee member for various microwave and semiconductor conferences, including the IMS and IEDM. In 1999, he was awarded a Creative Research Initiative Program by the Korean Ministry of Science and Technology with a nine-year term to develop new technologies in the interdisciplinary area of millimeter-wave electronics, MEMS, and biotechnology. He was the recipient of the Presidential Young Investigator Award from the Korean government in 2006.

Dong-il "Dan" Cho (M'88) received the B.S.M.E. degree from Carnegie-Mellon University, Pittsburgh, PA, in 1980, and the S.M. and Ph.D. degrees from Massachusetts Institute of Technology, Cambridge, in 1984 and 1987, respectively.

From 1987 to 1993, he was an Assistant Professor with the Mechanical and Aerospace Engineering Department, Princeton University, Princeton, NJ. Since 1992, he has been with the School of Electrical Engineering and Computer Science, Seoul National University, Seoul, Korea, where he is currently a Professor and the Director of the Automation and Systems Research Institute. He was the Director of the Microsystem Technology Center during 2002–2006 and the Chairman of the Korea MEMS Association during 2004–2007. He was an Associate Editor for the *IOP Journal of Micromechanics and Microengineering* and an Acting Associate Editor for the *ASME Transactions Journal of Dynamic Systems, Measurement, and Control*. He has been an Associate Editor for the *Journal of Micromechatronics* since 1999 and an Editorial Board Member for *Sensors and Materials* since 2003 and the *Journal of Micro-Nano Mechatronics* since 2005. He is the author or coauthor of more than 200 scientific articles in English. He is the holder/coholder of more than 70 patents. His research interests include microprocesses, inertial sensors, bioMEMS, and RF MEMS.

Prof. Cho was an Editor/Associate Editor for the JOURNAL OF MICROELECTROMECHANICAL SYSTEMS. He has been an Editor for the JOURNAL OF MICROELECTROMECHANICAL SYSTEMS since 2000. In 2008, he was the IPC Chair of the IFAC World Congress, which attracted 3800 paper submissions.